



POLITECNICO DI TORINO
Repository ISTITUZIONALE

Cinematic and Dynamic Modelling of Centerless Grinding

Original

Cinematic and Dynamic Modelling of Centerless Grinding / Priarone P.C.; Rizzuti S.; Settineri L.. - STAMPA. - (2011), pp. 141-152. ((Intervento presentato al convegno 9th Int. Conference on Advanced Manufacturing Systems and Technology, AMST 2011 tenutosi a Mali Losinj nel June 16-18 2011.

Availability:

This version is available at: 11583/2460384 since:

Publisher:

Prof. Elso Kuljanic

Published

DOI:

Terms of use:

openAccess

This article is made available under terms and conditions as specified in the corresponding bibliographic description in the repository

Publisher copyright

(Article begins on next page)

CINEMATIC AND DYNAMIC MODELLING OF CENTERLESS GRINDING

P. Priarone, S. Rizzuti, L. Settineri

Department of Production Systems and Business Economics, Politecnico di Torino

KEYWORDS: Cutting, Centerless grinding, Modelling

ABSTRACT. Chip removal and the formation of a round profile are complex questions in centerless grinding. The shape assumed by the part during every single instant of the machining operation depends essentially on its relative position with respect to the operating grinding wheel. This position is function of an elevated number of factors.

The aim of this paper is the determination of the profile resulting from a grinding operation, taking into account the original shape of the part, the machine, the tools and the contact between tools and part.

After an analysis of the pre-existing models, a new approach is proposed based on the discretization of the system in parallel planes that takes into account the deformability of the part axis, generated by the cutting forces and by the reaction forces of regulating wheel and workblade.

1 INTRODUCTION

Centerless grinding is a chip removal process in which the workpiece is not clamped, but it is just supported by a “V” formed by the regulating wheel, the grinding wheel and a workblade. A schematic picture of a centerless grinding machine is represented in Figure 1.

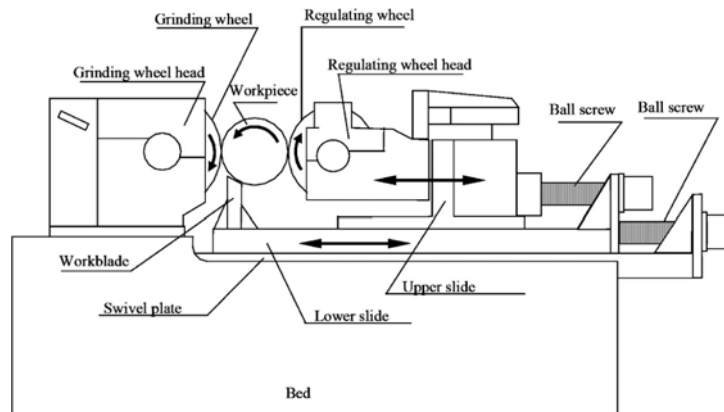


FIGURE 1. Scheme of the centerless grinding machine

This configuration is quite advantageous, since it allows a simple and easy load/unload operations with minimal interruption of the process.

On the other hand, the floating centre of the workpiece easily generates problems of roundness errors. Such errors given the particular configuration of the machine, produce a displacement of the part centre, that lead to an error regeneration mechanism.

Several researchers have studied the origin and evolution of the roundness errors in centerless grinding [1–4]. These researches have shown that geometric and dynamic causes can produce

instabilities. In particular, geometric instabilities are typical of centerless grinding and they are produced as a consequence of the geometric configuration of the machine, independent of the structural characteristics and the workpiece angular velocity. In addition, the compliance of the part can add dynamic effects to such phenomenon, limiting the geometric accuracy and the surface quality of the workpieces [5].

In this paper a simple model for the description of the centerless grinding process is presented, aimed at forecasting the geometrical error of the part, knowing the part characteristics and the process parameters.

2 PROPOSED MODEL

The models proposed in the literature do not allow an accurate study of the machine geometry, the main limitation being that they are mostly bidimensional [5,6 and ref. therein].

The proposed model is based on a geometrical representation of the tools, described as a surface in a 3D space, and on a discrete representation of the part shape, through a series of functions $r_w(\phi)$, that give, in form of cylindrical coordinates, the distance of the points of the part surface from a reference axis, in correspondence of some perpendicular sections, see Figure 2.

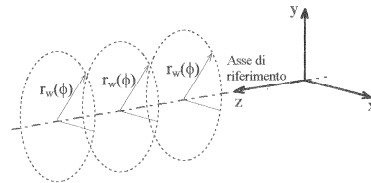


FIGURE 2. Part shape definition

The approach is to section the system with planes perpendicular to the part axis. On each plane is therefore possible to determine the position of the part axis, and therefore to compute the amount of material removed by the operating wheel. The part axis can undergo elastic deformation under the forces originated during machining.

The equations representing analytically the wheels and the workblade surfaces are computed in function of the position of the slides, to take into account the machine registration parameters.

Nonlinearities, given by the irregular part shape, the curvature of the wheels, the holonomic position constraints and the deformation of the part, make necessary a recursive computation.

The main feature of the model is the computation of the position assumed in every time instant by the part, with respect to the machine, taking into account for the part compliance.

2.1 GEOMETRICAL DEFINITION OF THE TOOLS

Several reference systems are used in the presented model, each one solid with one of the independently moving parts of the machine. In Figure 3 the reference systems are illustrated. To pass from one reference system to the other a set of transformation matrixes has been used.

The grinding wheel surface is computed as the surface generated by the revolution of the straight line representing the path of the diamond tool for the regeneration of the operating wheel. Being $O_{\rho}x_{\rho}y_{\rho}z_{\rho}$ the grinding wheel space, the grinding wheel surface equation is:

$$x_0^2 + y_0^2 = \left[\frac{z_0 - z_{0D_0}}{z_{0D_1} - z_{0D_0}} (x_{0D_1} - x_{0D_0}) + x_{0D_0} \right]^2 + \left[\frac{z_0 - z_{0D_0}}{z_{0D_1} - z_{0D_0}} (y_{0D_1} - y_{0D_0}) + y_{0D_0} \right]^2 \quad (1)$$

Where D_0 and D_1 are two points, with known coordinates, laying the straight path of the diamond tool.

With the same procedure, being $O_5x_5y_5z_5$ the regulating wheel space, the regulating wheel surface equation is:

$$x_5^2 + y_5^2 = \left[\frac{z_5 - z_{5D_0}}{z_{5D_1} - z_{5D_0}} (x_{5D_1} - x_{5D_0}) + x_{5D_0} \right]^2 + \left[\frac{z_5 - z_{5D_0}}{z_{5D_1} - z_{5D_0}} (y_{5D_1} - y_{5D_0}) + y_{5D_0} \right]^2 \quad (2)$$

Where D_0 and D_1 are two points, with known coordinates, on the straight path of the diamond tool for the regeneration of the regulating wheel

The workblade surface equation, being $O_2x_2y_2z_2$ the workblade space, is:

$$y_2 + x_2 \tan \theta - y_{2p} - x_{2p} \tan \theta \quad (3)$$

Where x_{2p} and y_{2p} are the coordinates of a P point on the blade surface, and θ the inclination angle of the blade surface with respect to the horizontal.

2.2 PART-TOOLS CONTACT

As for the contact points between the part and the regulating wheel and the workblade, they are computed for each part section with a recursive approach. With reference to Figure 3, the steps are the following:

- a first approximation of the angular position of the contact points is given, starting from the ideal geometry
- the provisional position of the centre O_w of the section is individuated
- the provisional position of the contact point with the regulating wheel is computed; if the angular position of the perpendicular to the wheel profile does not correspond to the ideal angles, there is no contact
- therefore new angular positions are assumed, based on the perpendiculars to the tool profiles and the process is repeated recursively until the error is small enough.

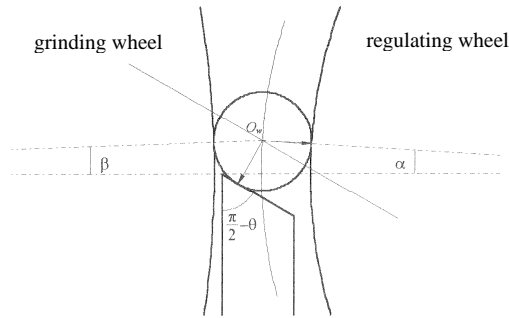


FIGURE 3. Determination of the part centre O_w , as intersection of the workblade profile and of the regulating wheel, translated respectively of r_{wb} and r_{rw}

Once the section centre O_w has been determined, its distance from the operating wheel is determined. The radius of the part is computed recursively for each part rotation and is the minimum between the value computed at revolution n and the value computed at revolution $n+1$. The grinding wheel is here assumed to be a circumference.

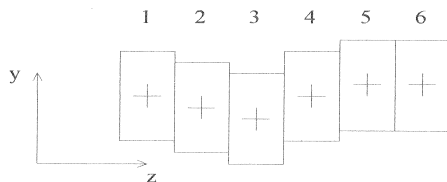
The part-tools contact points are computed at the same time for all the part sections perpendicular to the part axis. The model computes a matrix containing in each column the coordinates of the centres of each section and a vector with the inclination angles of the perpendiculars to the regulating wheel in the contact points.

2.3 PART DEFORMABILITY

The approach consists of computing the deformed part to calculate the constraint reactions needed to keep the part in that position and then to evaluate if such forces are applicable. If this is not the case, the algorithm modifies the part deformed shape and computes again the constraint forces in order to achieve an acceptable solution. This is recursively performed for each part rotation. Each step requires a new computation of the part sections' centres.

The correction of the axis curvature is then applied when the position of the centres is computed, by taking into consideration the radii obtained from the part geometry, increased by the local displacement between the part itself and the bearing surfaces.

In Figure 4 an example is reported of the computation of the characteristics of the forces and torques applied on the yz plane, based on the part deformation projected on the same plane. The same computation is performed on the xz plane. To simplify the example, the centre of each disk, in which we can imagine to partition the part, is considered at a unit distance, along the z axis, from the adjacent centres. The values of the elastic modulus E and of the inertia moment of the section I_y are taken, in this example, equal to 1.



$$\begin{array}{l}
 \frac{dy}{dz} \quad \quad \quad -1 \quad -1 \quad +2 \quad +1 \quad 0 \\
 \frac{d^2y}{dz^2} \quad \quad \quad 0 \quad +3 \quad -1 \quad -1 \\
 M_x \propto -\frac{d^2y}{dz^2} \quad 0 \quad 0 \quad -3 \quad +1 \quad +1 \quad 0 \\
 T_y = \frac{dM}{dz} \quad \quad 0 \quad 0 \quad -3 \quad 4 \quad 0 \quad -1 \quad 0 \\
 F_y = T_{i+1} - T_i \quad 0 \quad -3 \quad 7 \quad -4 \quad -1 \quad 1
 \end{array}$$

FIGURE 4. Simplified example of computation of the stress characteristics on the yz plane. M is the bending moment, T is the shear stress and F is the force

2.4 EXCHANGED FORCES

The cutting forces that are exchanged between the grinding wheel and the part during the machining depend on the chip section, on the cutting parameters, on the cutting fluid and on the characteristics of the grinding wheel and of the part.

In the presented model, the cutting force is computed using the well known cutting pressure method, i.e., by multiplying the cutting pressure by the chip section S :

$$F = K_s S \quad (4)$$

where $S = b h_m$ and $K_s = K_{s0} h^{-z}$, with K_{s0} specific cutting pressure, h chip thickness, h_m its mean value, b chip width and z experimental exponent. K_{s0} and z depend on the part material, cutting angles, tool material, cutting conditions in general. For further details, refer to [7].

The regulating wheel applies a tangential force to the part F_{rt} . If we neglect the tangential forces applied by the workblade, the torque generated by the cutting force must be equal and opposite to the torque generated by the tangential force applied by the regulating wheel, on all the n_s part sections:

$$\sum_{n_s} |F_{rt}| r_w = \sum_{n_s} |F_{wt}| r_w \quad (5)$$

Where F_{wt} is the tangential cutting force. We assume that the tangential cutting force in each section is equilibrated by the regulating wheel force acting on the same section. For those sections in which there is no contact with the regulating wheel, the F_{wt} is equally partitioned between the two adjacent sections.

2.5 RIGID BODY EQUILIBRIUM

If the resulting of the external forces applied to the part is external to the contact points with the workblade and regulating wheel, a rigid rotation is determined on the part, with a variation of the contact points until the force is again internal.

The modulus and z coordinate of the equivalent force to the forces normal to the workblade is given by:

$$R_{wb} = \sum_{i=1}^{n_s} (F_{wb})_i \quad (6)$$

$$z_R = \frac{\sum_{i=1}^{n_s} (F_{wb})_i \cdot z_i}{\sum_{i=1}^{n_s} (F_{wb})_i} \quad (7)$$

While the same quantities for the regulating wheel are given by:

$$R_{rw} = \sum_{i=1}^{n_s} (F_{rw})_i \quad (8)$$

$$z_R = \frac{\sum_{i=1}^{n_s} (F_{rw})_i \cdot z_i}{\sum_{i=1}^{n_s} (F_{rw})_i} \quad (9)$$

2.6 SHAPE VARIATIONS PROPORTIONAL TO THE FORCES

For each section of the part, the displacement with respect to the adjacent sections is computed by using a set of stiffness parameters contained in a vector k_{shape} . As an example, the rigidity parameters relevant to the case of an internal section displacement are shown in the following Figure 5. In this particular example, we obtain: $k_{shape} > 6EI/\Delta z^3$.

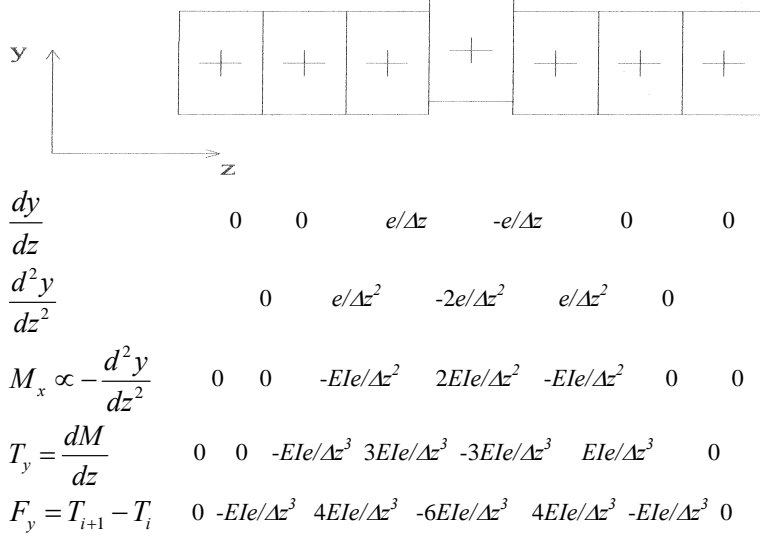


FIGURE 5. Deformation forces due to a displacement e of an internal section of the part

When the cutting forces are also included in the balance, k_{shape} must be further increased. A displacement e of a part section from the workblade produces an increase of the deformation forces that push that section towards the workblade, but produces as well a variation of the normal machining forces:

$$\Delta F_{wn} = -\varepsilon' \cdot k_{wn} \cdot e \quad (10)$$

This variation affects the forces exchanged with the workblade according to the equation:

$$F_{wb} = (\Delta F_{wn} \cos(\beta), \Delta F_{wn} \sin(\beta)) \cdot (-\sin(\alpha), -\cos(\alpha)) \frac{1}{\cos(\vartheta - \alpha)} \approx 0.01 \cdot k_{wn} \cdot e \quad (11)$$

The tangential machining forces, on the other hand, undergo the following variation:

$$\Delta F_{wt} = -\varepsilon' \cdot k_{wt} \cdot e \quad (12)$$

This variation affects the forces exchanged with the workblade according to the equation:

$$F_{wb} = (\Delta F_{wt} (\sin(\beta) - \sin(\alpha)), \Delta F_{wt} (-\cos(\beta) - \cos(\alpha))) \cdot (-\sin(\alpha), -\cos(\alpha)) \frac{1}{\cos(\vartheta - \alpha)} \approx -0.2 \cdot k_{wt} \cdot e \quad (13)$$

A displacement e of a part section from the regulating wheel produces a variation of the normal machining forces:

$$\Delta F_{wn} = (1 - \varepsilon) \cdot k_{wn} \cdot e \quad (14)$$

This variation affects the forces exchanged with the workblade according to the equation:

$$F_{wb} = (\Delta F_{wn} \cos(\beta), \Delta F_{wn} \sin(\beta)) \cdot (\cos(\theta), -\sin(\theta)) \frac{1}{\cos(\theta - \alpha)} \approx k_{wn} \cdot e \quad (15)$$

The tangential machining forces, on the other hand, undergo the following variation:

$$\Delta F_{wt} = (1 - \varepsilon) \cdot k_{wt} \cdot e \quad (16)$$

This variation affects the forces exchanged with the workblade according to the equation:

$$F_{wb} = (\Delta F_{wt} (\sin(\beta) - \sin(\alpha)), \Delta F_{wt} (-\cos(\beta) - \cos(\alpha)) \cdot (\cos(\theta), -\sin(\theta))) \frac{1}{\cos(\theta - \alpha)} \approx k_{wt} \cdot e \quad (17)$$

The variations of Δr_{wb} and Δr_{rw} generate a transversal displacement of each part section that will affect, in the next iteration, the value of the deformation forces of the next sections. These last will therefore undergo a displacement, to compensate such force variation.

We can introduce the terms $\Delta \Delta r_{wb3}$ and $\Delta \Delta r_{rw3}$, computed based on the influence of the displacement of the next sections; if the distances $\Delta \Delta r_w$, of all the n_s sections, and their variations are gathered in vectors of length n_s , the elements $\Delta \Delta r_{wb3}$ and $\Delta \Delta r_{rw3}$ can be computed at the same time with the equation:

$$\{\Delta \Delta r_{wb3}\} = [C_3] \max(-\{\Delta r_{wb}\}, \{\Delta \Delta r_{wb1}\} + \{\Delta \Delta r_{wb2}\}) \quad (18)$$

$$\{\Delta \Delta r_{rw3}\} = [C_3] \max(-\{\Delta r_{rw}\}, \{\Delta \Delta r_{rw1}\} + \{\Delta \Delta r_{rw2}\}) \quad (19)$$

Where in the matrix C_3 , the generic term i - j th represents the influence on section i of the displacement of section j .

The first column of matrix C_3 contains the terms affecting the shearing of the first section on all the others, while the elements of the second column are referred to the displacement of the second section, and so on. Therefore, if we consider:

$$K_0 = \frac{EI}{\Delta z^3} \quad (20)$$

We obtain:

$$[C_3] = \frac{1}{2} \begin{bmatrix} 0 & 2K_0 & -K_0 & 0 & 0 & 0 & 0 \\ 2K_0 & 0 & 4K_0 & -K_0 & 0 & 0 & 0 \\ -K_0 & 4K_0 & 0 & 4K_0 & -K_0 & 0 & 0 \\ 0 & -K_0 & 4K_0 & 0 & 4K_0 & -K_0 & 0 \\ 0 & 0 & -K_0 & 4K_0 & 0 & 4K_0 & -K_0 \\ 0 & 0 & 0 & -K_0 & 4K_0 & 0 & 2K_0 \\ 0 & 0 & 0 & 0 & -K_0 & 2K_0 & 0 \end{bmatrix} / K_0 \quad (21)$$

As a conclusion, if we put together the three variations, we obtain:

$$\Delta r_{wb} = \max(0, \Delta r_{wb} + \Delta \Delta r_{wb1} + \Delta \Delta r_{wb2} + \Delta \Delta r_{wb3}) \quad (22)$$

$$\Delta r_{rw} = \max(0, \Delta r_{rw} + \Delta \Delta r_{rw1} + \Delta \Delta r_{rw2} + \Delta \Delta r_{rw3}) \quad (23)$$

3 SIMULATION TESTS

Several simulation tests have been performed to study the effects of the geometrical machine set up on the final part shape.

The simulation tests have been first performed by introducing a sinus disturbance on the contact position of the part with the operating wheel. This test has been carried out to test the model reaction to a disturbance that can come from an eccentricity of the rotation axis, or from a mass disequilibrium generating a tool vibration. The goal of the simulation is to measure the effects of these disturbances on the roundness error of the part and on the amplitude of the waviness of the final profile, in order to understand when the errors can be compensated or if they are self-regenerating.

To this purpose, we define the ratio between the frequency of the disturbance and the rotational speed of the part:

$$k = \frac{N_g}{N_w} \quad (24)$$

The results of these first simulations are reported in Tables 1 and 2, where the roundness errors, the order and amplitude of the main harmonic as a function of the k coefficient, are reported. In the tables, k_{max} is the order of the larger harmonic, among those forming the part profile, while $a(k_{max})$ is its amplitude. Table 1 refers to a disturbance with amplitude 1 μm , while Table 2 refers to a disturbance with amplitude 10 μm .

TABLE 1. Roundness error and characteristics of the main harmonic as a function of k in the case of a disturbance with amplitude 1 μm

k	$h_t [\mu\text{m}]$	k_{max}	$a(k_{max}) [\mu\text{m}]$		k	$h_t [\mu\text{m}]$	k_{max}	$a(k_{max}) [\mu\text{m}]$
0	0.54	3÷5÷7	0.1		12	2.03	12	0.6
3.5	1.76	7	0.5		12.5	1.25	25	0.25
4	1.53	4	0.5		13	2.30	13	0.8
4.5	2.17	5	0.6		13.5	5.21	13	1.3
5	2.20	5	0.7		14	1.88	14	0.6
5.5	3.94	5	1.3		14.5	0.94	29	0.2
6	2.11	6	0.6		15	2.01	15	0.8
6.5	2.35	7	0.5		15.5	6.03	15	1.3
7	2.28	7	0.7		16	1.94	16	0.7
7.5	3.77	7	1.2		16.5	0.96	33	0.2
8	1.89	8	0.5		17	1.85	17	0.7
8.5	1.52	17	0.3		17.5	6.33	17	1.5
9	2.91	9	1.3		18	2.12	18	0.81
9.5	2.79	9	0.6		18.5	1.10	37	0.2
10	1.57	10	0.6		19	2.03	19	0.7
10.5	1.26	21	0.3		19.5	6.76	20	0.5
11	2.45	11	0.8		20	2.03	20	0.8
11.5	5.37	11	1.4					

TABLE 2. Roundness error and characteristics of the main harmonic as a function of k in the case of a disturbance with amplitude $10\mu\text{m}$

k	h_t [μm]	k_{max}	$a(k_{max})$ [μm]		k	h_t [μm]	k_{max}	$a(k_{max})$ [μm]
0	0.54	3÷5÷7	0.1		11.5	11.82	23	3.5
3.5	31.94	7	13.0		12	13.64	12	6.5
4	11.87	4	5.0		12.5	6.23	25	2.5
4.5	8.29	9	2.5		13	20.78	13	10.0
5	48.86	5	25.0		13.5	12.11	27	3.0
5.5	19.04	11	8.0		14	13.20	14	6.2
6	12.77	6	5.6		14.5	5.72	29	2.3
6.2	6.02	6	1.2		15	16.90	15	8.0
6.5	10.32	13	1.8		15.5	10.75	31	2.9
6.7	12.83	7	3.5		16	14.08	16	6.9
7	44.87	7	22.0		16.5	6.07	33	2.3
7.5	15.35	15	5.0		17	14.71	17	7.0
8	11.20	8	5.5		17.5	11.66	35	2.9
8.5	10.13	17	2.2		18	17.71	18	8.5
9	26.55	9	13.0		18.5	6.63	37	2.4
9.5	15.58	19	4.5		19	15.34	19	7.3
10	11.91	10	5.6		19.5	12.11	39	3.1
10.5	7.65	21	2.3		20	16.48	20	8.2
11	21.12	11	10.0		20.5	5.64	41	2.3

Further simulations have been run, introducing a sinusoidal disturbance in the contact position with the regulating wheel. Such simulations are not reported for lack of space. Interesting results have been obtained in the simulation of the detachments of the part from the workblade and the regulating wheel. As a consequence of such detachments, the average part radius is not constant along the part length and in some sections of the part we obtain a two-lobes profile.

Figure 6 reports the difference from the linear behaviour of the radii along the part length, referred to two different working heights. Figures 7 and 8 show the results on the profile analysis carried out on two sections of the part that during the simulation were detached from the tools. The difference from the ideal profile is shown, and the corresponding amplitudes a_k of the harmonics obtained through a profile Fourier analysis.

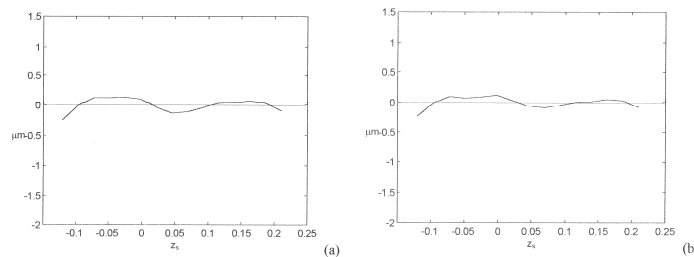


FIGURE 6. Difference from linearity along the part axis for the two working heights above centres $h=0$ mm (a) and $h=10$ mm (b). The slide rotation φ_l , corresponds to 10°

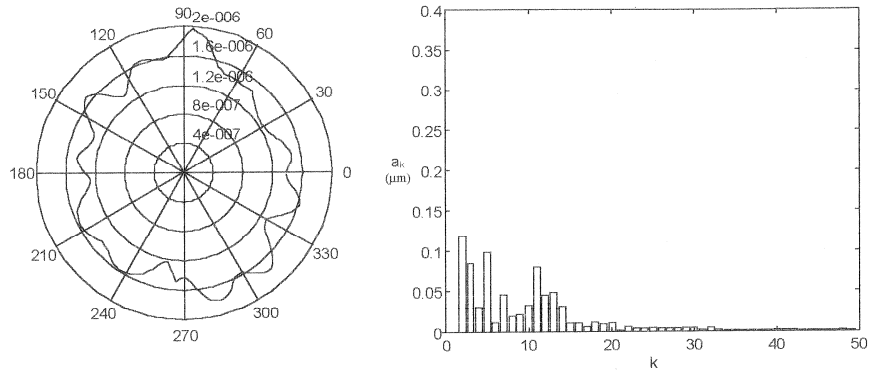


FIGURE 7. Roundness error in section 2 of the part and corresponding amplitudes a_k of the harmonics: the main harmonic is of order 2

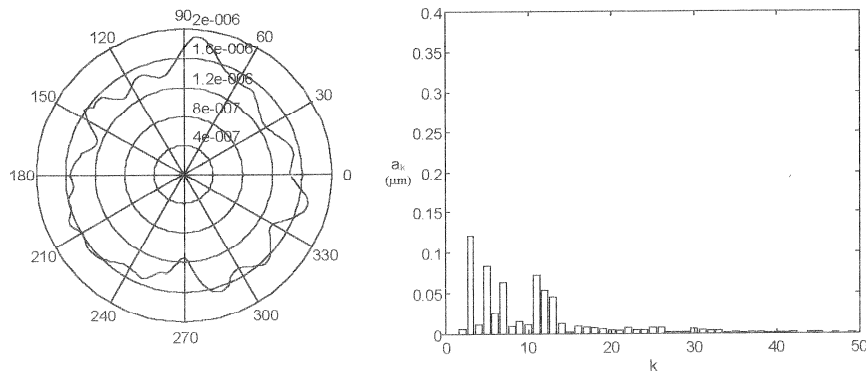


FIGURE 8. Roundness error in section 3 of the part and corresponding amplitudes a_k of the harmonics: the main harmonic is of order 3

4 EXPERIMENTAL RESULTS

The main experimental conditions are reported in Table 3. Four samples for each parameter combination have been machined, and the average diameter of each section are reported in Figures 9 and 10, that represent the difference between the real and the ideal value of the part radius, corresponding to $\varphi_1 = \varphi_5 = \varphi_6 = 0^\circ$. In these Figures the results of some experimental tests vs. the results of the corresponding simulations in terms of average value of 4 repetitions are reported. The figures show that the slide rotational angle φ_1 , the regulating wheel registration angle φ_5 and the regulating wheel regeneration angle φ_6 , they all affect the part average radius along the part length. The differences in terms of average radius between the most external sections can also be found in Table 4.

TABLE 3. Main parameters of the experimental tests

Machine	BMS 101/001
Operating wheel diameter	440 mm
Regulating wheel diameter	300 mm
External part diameter	25 mm
Internal part diameter	13 mm
Part length l_p	280 mm
Part material	Carbon Steel AISI 1040
Number and thickness of considered sections	$n_s = 13; 20$ mm
Slide registration angle φ_1	$-10'; 0'; 10'; 20'$
Regulating wheel registration angle φ_5	$0.5^\circ; 1.0^\circ; 1.5^\circ$
Regulating wheel regenerating angle φ_6	$0^\circ; 1^\circ$
Height over the centres of the part h	$0 \div 10$ mm
Number of repetitions for each parameters' set	4

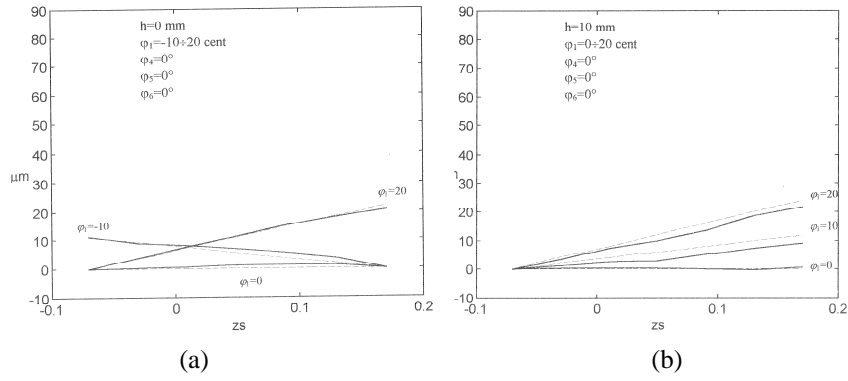


FIGURE 9. Average part radius along the axis, for three values of the rotation angle of the slide φ_1 ; height above centers $h = 0$ mm (a) and 10 mm (b). Continuous lines represent the experiments, dotted lines represent the simulations

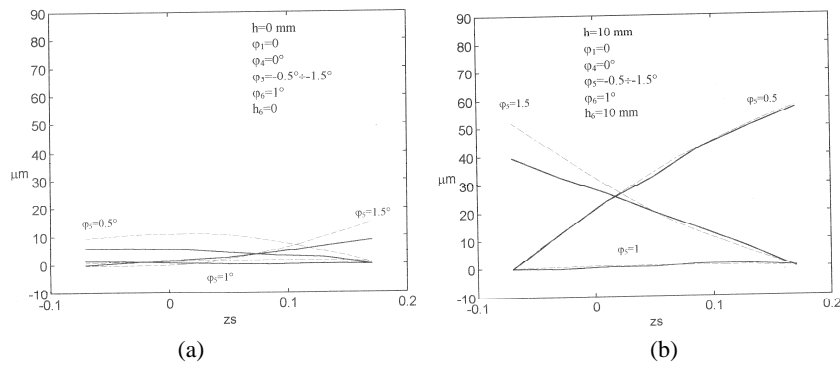


FIGURE 10. Average part radius along the axis, for three values of the rotation angle of the regulating wheel φ_5 ; height above centers $h = 0$ mm (a) and 10 mm (b). Continuous lines represent the experiments, dotted lines represent the simulations

TABLE 4. Comparison of the experimental and simulated radius differences between the most external sections

Conditions	Experimental $r_{\theta}(13)-r_{\theta}(1)$	Simulated $r_{\theta}(13)-r_{\theta}(1)$
$h = 0 \text{ mm}; \varphi_1 = 20^\circ; \varphi_5 = \varphi_6 = 0^\circ$	21 μm	21.8 μm
$h = 10 \text{ mm}; \varphi_1 = 20^\circ; \varphi_5 = \varphi_6 = 0^\circ$	22 μm	23.8 μm

5 CONCLUSION

In this paper a numerical simulation method of the centerless grinding process has been presented. The method allows to forecast the part surface geometry as the geometrical process parameters vary.

The introduction in the model of all the geometrical set up parameters of the grinding machine and of the elastic response of the part allows to obtain satisfactory results in terms of shape error evaluation on the machined parts.

The model allows to forecast the formation of the shape defects that have geometrical origin, such as taper angles, concavity, number of lobes in the final part. Further, the roundness error can be forecast.

As for the errors that have dynamical origin, the model evaluates the interference of the part geometry with disturbances having a pre-defined law, without taking into account the problems regarding the self-excited vibrations of the system.

REFERENCES

1. Gurney, J.P., (1965), An analysis of centerless grinding, ASME Journal of Engineering for Industry, Vol. 87, 163–174.
2. Rowe, W.B., Koenigsberger, F., (1964), The ‘‘work-regenerative’’ effect in centerless grinding, International Journal of Machine Tool Design and Research, Vol. 4, 175–187.
3. Furukawa, Y., Miyashita, M., Shiozaki, S., (1970), Vibration analysis and work-rounding mechanism in centerless grinding, International Journal of Machine Tool Design and Research, Vol. 11, 145–175.
4. Garitaonandia, I., Fernandes, M.H., Albizuri, J., Hernandez, J.M., Barrenetxea, D., (2010), A new perspective on the stability study of centerless grinding process, International Journal of Machine Tools and Manufacture, Vol. 50\2, 165-173.
5. Miyashita, M., Hashimoto, F., Kanai, A., (1982), Diagram for selecting chatter free conditions of centerless grinding, Annals of the CIRP Vol. 31\1, 221–223.
6. Garitaonandia, I., Fernandes, M.H., Albizuri, J., (2008), Dynamic model of a centerless grinding machine based on an updated FE model, International Journal of Machine Tool and Manufacture, Vol 48, 832-840.
7. Kalpakjian, S., Schmid, S., (2010), Manufacturing Engineering & Technology, Prentice Hall, U.S.A.